The WindSat Spaceborne Polarimetric Microwave Radiometer: Sensor Description and Early Orbit Performance

Peter W. Gaiser, *Senior Member, IEEE*, Karen M. St. Germain, *Senior Member, IEEE*, Elizabeth M. Twarog, Gene A. Poe, *Member, IEEE*, William Purdy, Donald Richardson, Walter Grossman, *Member, IEEE*, W. Linwood Jones, *Fellow, IEEE*, David Spencer, Gerald Golba, *Member, IEEE*, Jeffrey Cleveland, Larry Choy, Richard M. Bevilacqua, and Paul S. Chang, *Senior Member, IEEE*

***Abstract*—The global ocean surface wind vector is a key parameter for short-term weather forecasting, the issuing of timely weather warnings, and the gathering of general climatological data. In addition, it affects a broad range of naval missions, including strategic ship movement and positioning, aircraft carrier operations, aircraft deployment, effective weapons use, underway replenishment, and littoral operations. WindSat is a satellite-based multifrequency polarimetric microwave radiometer developed by the Naval Research Laboratory for the U.S. Navy and the National Polar-orbiting Operational Environmental Satellite System Integrated Program Office. It is designed to demonstrate the capability of polarimetric microwave radiometry to measure the ocean surface wind vector from space. The sensor provides risk reduction for the development of the Conical Microwave Imager Sounder, which is planned to provide wind vector data operationally starting in 2010. WindSat is the primary payload on the Department of Defense Coriolis satellite, which was launched on January 6, 2003. It is in an 840-km circular sun-synchronous orbit. The WindSat payload is performing well and is currently undergoing rigorous calibration and validation to verify mission success.**

***Index Terms*—Ocean surface winds, remote sensing, WindSat.**

I. Introduction

THE GLOBAL ocean surface wind vector (wind speed and direction) field provides essential environmental information. It is critical data for short-term weather forecasts and warnings, nowcasting, climatology, and oceanography studies. Ocean surface wind field measurements support basic research in air–sea interaction, tropical cyclogenesis, ocean circulation, and atmospheric convection. In addition, the wind vector affects a broad range of naval operations including strategic ship movement and positioning, aircraft carrier operations, aircraft deployment, underway replenishment, and littoral operations. Historically, spaceborne scatterometers such as the National Aeronautics and Space Administration (NASA) NSCAT and SeaWinds instruments have provided global ocean surface wind vector information. However, there have never been a sufficient number of these sensors simultaneously operational, in the proper orbits, to satisfy revisit and coverage requirements necessary for full utilization in operational meteorological applications.

Passive spaceborne microwave radiometry has a strong heritage based largely on the Special Sensor Microwave/Imager (SSM/I) series of instruments, operated by the Defense Meteorological Satellite Program (DMSP). Over the past 15 years, seven SSM/Is have successfully provided reliable passive microwave data for retrieving environmental parameters such as wind speed, sea ice concentration and age, and integrated atmospheric water vapor [1]–[3]. One parameter that has not been provided by microwave radiometers is the wind direction. However, analysis of SSM/I data has revealed a wind direction dependence in the vertical and horizontal polarizations, which has been confirmed by modeling and aircraft measurements [4], [5]. But, the vertical and horizontal channels do not contain enough information to unambiguously retrieve the wind direction, because the wind direction dependencies, for both vertical and horizontal polarizations, are even functions about relative wind directions of 0° and 180°.

Recent research in polarimetric radiometry modeling and measurements has demonstrated that usable wind direction information can be obtained by combining the vertical and horizontal polarizations with the cross correlation of those two polarizations [4]–[11]. The cross-correlation terms represent the third and fourth parameters of the modified Stokes vector, defined [12] as

$$I_s = \begin{bmatrix} I \\ Q \\ U \\ V \end{bmatrix} = \begin{bmatrix} T_{\mathrm{v}} \\ T_{\mathrm{h}} \\ T_{45} - T_{-45} \\ T_{\mathrm{lc}} - T_{\mathrm{rc}} \end{bmatrix} = \begin{bmatrix} \langle E_{\mathrm{v}} E_{\mathrm{v}}^* \rangle \\ \langle E_{\mathrm{h}} E_{\mathrm{h}}^* \rangle \\ 2\,\mathrm{Re}\,\langle E_{\mathrm{v}} E_{\mathrm{h}}^* \rangle \\ 2\,\mathrm{Im}\,\langle E_{\mathrm{v}} E_{\mathrm{h}}^* \rangle \end{bmatrix}. \quad (1)$$

In this definition, T_{v}, T_{h}, T_{45}, T_{-45}, T_{lc}, and T_{rc} represent brightness temperatures (radiances) at vertical, horizontal,

Manuscript received February 12, 2004; revised June 16, 2004. The WindSat program is supported by the U.S. Navy (N61) and the NPOESS Integrated Program Office.

P. W. Gaiser, K. M. St. Germain, E. M. Twarog, W. Purdy, D. Spencer, G. Golba, J. Cleveland, L. Choy, and R. M. Bevilacqua are with the Naval Research Laboratory, Washington, DC 20375 USA (e-mail: peter.gaiser@nrl.navy.mil).

G. A. Poe is with the Naval Research Laboratory, Monterey, CA 93943 USA.

D. Richardson is with Computational Physics, Inc., Springfield, VA 22151 USA.

W. Grossman is with Applied Systems Engineering, Inc., Gambrills, MD 21054 USA.

W. L. Jones is with Microwave Remote Sensing Consultants, Cocoa Beach, FL 32931 USA.

P. S. Chang is with the National Oceanic and Atmospheric Administration, National Environmental Satellite, Data, and Information Service, Office of Research and Applications, Camp Springs, MD 20746 USA.

Digital Object Identifier 10.1109/TGRS.2004.836867

Fig. 1. WindSat payload in the thermal/vacuum chamber. The cold sky reflector has been removed in this picture.

$+45°$, $-45°$, left-hand circular, and right-hand circular polarizations, respectively. The Stokes vector provides a full characterization of the electromagnetic signature of the ocean surface and the independent information needed to, at least in principle, uniquely determine the wind direction.

These advances come at a critical time for the development of future environmental remote sensing systems. Through its Integrated Operational Requirements Document (IORD) 1, of March 14, 1996, the National Polar-orbiting Operational Environmental Satellite System (NPOESS) program is required to provide, over a period of at least ten years, for remotely sensing, storing, and disseminating real-time global and regional environmental data in support of Department of Defense (DoD) and Department of Commerce (DoC) operational requirements. An important element of that capability is the accurate measurement of the ocean surface wind vector. Based on the aforementioned results and studies, NPOESS has opted to fulfill the wind vector measurement requirement using polarimetric microwave radiometry. That is, the NPOESS Conical Microwave Imager and Sounder (CMIS), which is the NPOESS replacement for the DMSP SSM/I program, will incorporate polarimetric capability. This would allow the global ocean wind vector, along with the many other environmental parameters now obtained by SSM/I, to be obtained with a single instrument.

WindSat is the first spaceborne polarimetric microwave radiometer. Its objective is to measure the partially polarized emission from the ocean surface and, therefore, test and fully evaluate the viability of using passive polarimetric radiometry to retrieve the ocean surface wind vector. The WindSat payload, shown in Fig. 1, was designed, built, and tested at the Naval Research Laboratory (NRL) in Washington, DC, under sponsorship from the United States Navy and NPOESS. The WindSat radiometer operates in discrete bands at 6.8, 10.7, 18.7, 23.8, and 37.0 GHz. The 10.7-, 18.7-, and 37.0-GHz channels are fully polarimetric, while the 6.8- and 23.8-GHz channels are dual polarized only (vertical and horizontal). The WindSat instrument was successfully launched on board the DoD Coriolis satellite mission on January 6, 2003, into an 840-km sun-synchronous orbit with the local time of the ascending node (LTAN) at 17:59. The instrument is currently operating nominally. WindSat calibration and the development of wind vector retrievals are ongoing work at the time of writing. This paper describes the WindSat mission and sensor design, describing the unique aspects of the development of a spaceborne polarimetric microwave radiometer. The paper then presents the early orbit radiometer performance.

II. Requirements

A. Performance Requirements

The requirements for wind vector are typically broken down into requirements for Sea Surface Wind Speed (SSWS) and Sea Surface Wind Direction (SSWD). The WindSat top-level performance goals are summarized in Table I and compared with NPOESS IORD and the CMIS.

In addition to the required ocean surface wind speed and direction, the WindSat system will provide a host of secondary ocean-scene environmental data products. These products are: column integrated cloud liquid water (CLW), column integrated precipitable water (PW), and sea surface temperature (SST). The WindSat data also have potential applications for land and ice data products.

The WindSat spatial resolution requirement represents a compromise between meeting the NPOESS CMIS/IORD requirement, staying within the allowable launch vehicle envelope, and minimizing risk and cost associated with postlaunch reflector antenna deployment. WindSat does not have operational requirements driving the swath width or global coverage. Rather, the WindSat mission is designed so that a portion of the swath is sampled in both the forward and aft viewing directions. This two-look capability provides an evaluation of the wind direction retrieval accuracy under single- and two-look operations. In this manner, an assessment will be made of the necessity of such a configuration for an operational system.

B. Sensor Requirements

The WindSat design team performed a radiometric sensitivity analysis to derive all key WindSat system requirements to meet the wind speed and direction performance goals. In support of this effort, NRL developed a two-scale model of the ocean surface emission and scattering [11], [13] and validated it using data collected from an aircraft platform. The model was also validated with SSM/I data and surface-based measurements. Following the model development, software was developed at NRL to simulate the effects of WindSat system errors on the data. The simulator accounts for system errors introduced by onboard alignment and pointing errors, calibration load uncertainties, radiometer nonlinearity, channel-to-channel imbalances, physical temperature uncertainty, and environmental and random noise.

TABLE I
WINDSAT PERFORMANCE REQUIREMENTS

Parameter	Accuracy			Range			Spatial Resolution		
System	WindSat	CMIS	IORD	WindSat	CMIS	IORD	WindSat	CMIS	IORD
Wind Speed	± 2 m/s or 20%			3-25 m/s			~30 km	20 km	
Wind Direction	± 20 ° (3-25 m/s)			0 - 360°			~30 km	20 km	

TABLE II
PERFORMANCE REQUIREMENTS FOR WINDSAT. THE ABSOLUTE ACCURACY REQUIREMENTS ARE 0.75 K FOR THE VERTICAL AND HORIZONTAL POLARIZATIONS AND 0.25 K FOR THE THIRD AND FOURTH STOKES PARAMETERS. THE NEDT REQUIREMENTS ASSUME SCENE BRIGHTNESS TEMPERATURE OF 250 K

Freq, GHz	Polarization	BW, MHz	Absolute Accuracy, K	Integration Time, msec	NEDT, K IFOV	Dynamic Range, K
6.8	V,H	125	0.75	5.00	0.63	3-330
10.7	V,H,U,4	300	0.75/0.25	3.93	0.44	3-330
18.7	V,H,U,4	750	0.75/0.25	2.19	0.44	3-330
23.8	V,H	500	0.75	1.63	0.60	3-330
37.0	V,H,U,4	2000	0.75/0.25	1.08	0.42	3-330

TABLE III
WINDSAT SCAN AND SAMPLING REQUIREMENTS

Parameter	Requirement	Channels Affected
Along Scan Sampling	Spatial Nyquist Sampling	All
Along Track Sampling	Contiguous Sampling	37 GHz
	Nyquist Sampling	All but 37 GHz
Mapping Accuracy	4 km (1/2 smallest footprint)	All
Scan Azimuth Angle Control	Control < 0.15°	All
Viewing	Fore and Aft	All
Swath Width	Maximum Feasible	All

TABLE IV
WINDSAT ANTENNA PERFORMANCE REQUIREMENTS. THE POLARIZATION PURITY REFERS TO RESIDUAL COUPLING AFTER CORRECTION FOR ANTENNA CROSS POLARIZATION

Parameter	Requirements	Channels Affected
Beam Efficiency	95%	All
Polarization Purity	Residual Coupling -30dB	Polarimetric Bands
	Residual Coupling ñ23 dB	Dual-Polarized Bands
Horizontal Spatial Resolution	30 Km Goal	Composite
Polarization Rotation Angle	Knowledge < 0.05° Bias and Random	Dual and Third Stokes
	Alignment of ± 1°	Dual and Third Stokes
Earth Incidence Angle	Nominal Fixed EIA between 50° and 55°	All
	Knowledge < 0.05° Bias and Random	All
	Maximum Variation 0.25°	All
Beam Coincidence	Ability to overlay, reregister and average beams	All

Using the simulator, the design team generated a large database of "observations" that could be run through data correction and wind retrieval algorithms, resulting in a comparison of original versus retrieved geophysical parameters. Using an iterative process, the design team partitioned the allowable errors and determined what knowledge of these errors was necessary for effective correction to be possible. The sensitivity analysis derived the required noise-equivalent differential temperature (NEDT) based on the effective field of view (EFOV) after averaging multiple pixels together. This was converted to single-pixel or instantaneous field of view (IFOV) based on design integration times and a scene temperature of 250 K. The top-level requirements for radiometers, sampling, and antenna are shown in Tables II–IV, respectively.

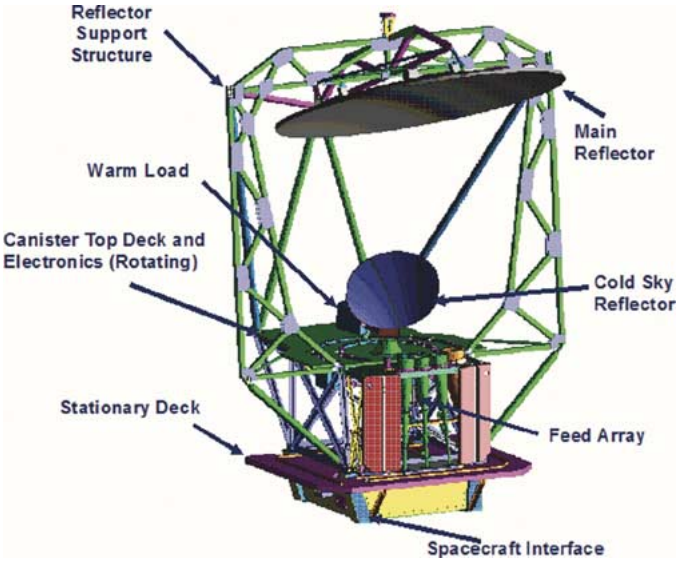

Fig. 2. Drawing of the WindSat payload with major components labeled.

III. Instrument Description

WindSat is the world's first spaceborne microwave polarimeter (high-precision passive microwave imager) that measures the partially polarized energy emitted, scattered, and reflected from the earth's atmosphere and surfaces. The instrument operates with 22 discrete channels covering five widely spaced frequency bands. For the polarimetric bands (10.7, 18.7, and 37.0 GHz), three dual-polarization feed horns are used: V/H, $+45°/-45°$ linear, and left/right circular. The third and fourth Stokes parameters are formed by taking the brightness temperature difference between the $+45°$ and $-45°$ polarizations, and the left-hand and right-hand circular polarizations, respectively, as described in (1).

WindSat comprises four major subsystems: antenna/calibration subsystem (spinning and nonspinning), receiver subsystem (spinning), data handling subsystem (spinning and nonspinning), and structural/thermal subsystem (spinning and nonspinning). Fig. 2 depicts a conceptual drawing of WindSat with the major elements indicated. The subsystems are described here.

A. Antenna/Calibration Subsystem

The antenna/calibration subsystem consists of the main reflector, 11 feed horns, a warm calibration load, and a cold sky calibration reflector. The main reflector is a 1.8-m diameter offset parabolic reflector fabricated of graphite epoxy with vapor deposited aluminum (VDA) coating. The reflector, along with the majority of the sensor hardware, rotates at a nominal rate of 31.6 r/min. A composite truss with a very low coefficient of thermal expansion (CTE) supports the main reflector. The 11 dual-polarized corrugated feedhorns provide the initial frequency channelization of the system and polarization splitting via orthomode transducers (OMT). The circularly polarized feeds use polarizers based on the design of Simmons [14]. However, the WindSat polarizers achieve the necessary phase shift with tuning screws rather than dielectric vanes.

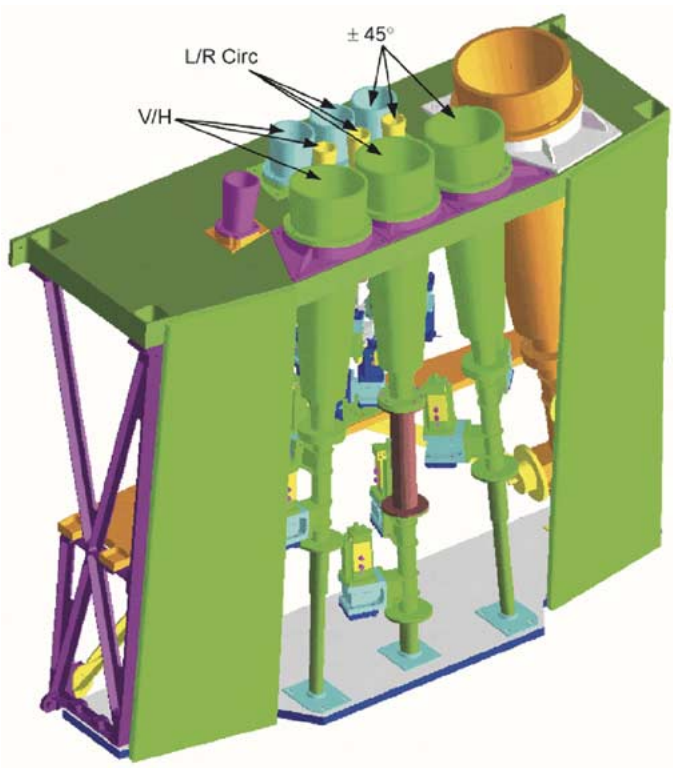

Fig. 3. WindSat feedbench. Green horns are 10.7 GHz; blue horns are 18.7 GHz; yellow horns are 37.0 GHz; the orange horn is 6.8 GHz; and the magenta horn is 23.8 GHz.

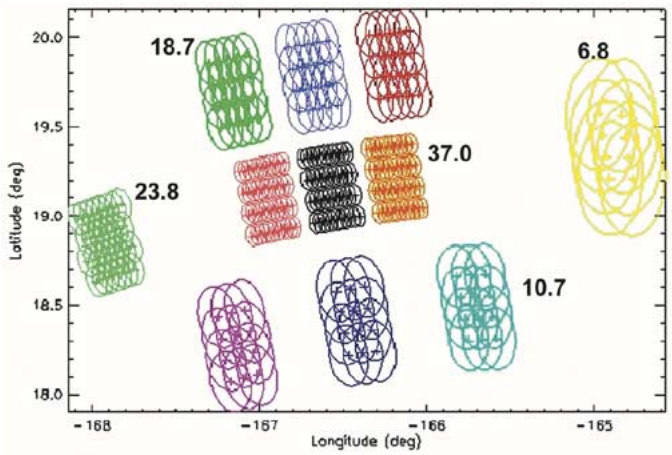

Fig. 4. WindSat antenna footprints projected on the surface of the earth. The figure shows a subset of four scans. Note that all frequencies are Nyquist sampled in the along-scan direction. One can see the relative sampling rate among the frequency bands.

The feedhorns are arranged on the feedbench as shown in Fig. 3, with the 37-GHz circularly polarized feed at the focal point of the reflector. This feedhorn configuration results in earth projected beams as shown in Fig. 4. Note that the earth incidence angle (EIA) is not the same for all frequencies. The nominal range is approximately 50° to 55°, which is consistent with the NPOESS CMIS concept, the aircraft data collected, and the SSM/I heritage. Horns within the same frequency band are arranged on the feedbench to ensure that the beams have the same EIA, but will be displaced from one another along the scan.

TABLE V
ANTENNA PARAMETERS. (vh) REFERS TO THE VERTICAL/HORIZONTAL FEED. (45) REFERS TO THE $\pm 45^\circ$ FEED, AND (cp) REFERS TO THE LEFT- AND RIGHT-CIRCULAR FEED. THE BEAMWIDTH IS THE AVERAGE FOR THE IFOV OVER THE E/H PLANES AND BANDWIDTH. THE EIA ASSUMES A NOMINAL SPACE VEHICLE ALTITUDE OF 830 km

Feed	Band	Pol	3 dB BW	Main BE	EIA	PRA
1	6.8	vh	1.78	96.80	53.5335	-0.0990
2	10.7	vh	1.13	97.80	49.9090	-0.0400
3	10.7	45	1.13	97.70	49.9272	0.4980
4	10.7	cp	1.13	98.80	49.9287	0.0000
5	18.7	vh	0.65	97.40	55.3510	0.0980
6	18.7	45	0.65	97.30	55.3526	0.3107
7	18.7	cp	0.65	98.30	55.3293	0.0000
8	23.8	vh	0.54	96.20	53.0007	4.9688
9	37.0	vh	0.33	96.90	53.0054	-0.3032
10	37.0	45	0.33	97.10	52.9939	0.3580
11	37.0	cp	0.33	98.80	53.0116	0.0000

The WindSat antenna/calibration subsystem configuration allows an end-to-end radiometer calibration once per revolution and presents no blockage of the scene energy by feeds or structure. This latter feature results in high beam efficiency. However, the polarization purity of an offset parabolic dish is typically too low for a polarimetric radiometer. Polarization purity is defined as the percentage of energy received in the desired polarization relative to the total energy received. The polarization purity can be improved by increasing the f/D ratio, where f is the focal length and D is the diameter of the parent parabola. For WindSat, increasing the f/D ratio is not feasible because of the size and mechanical implications. The other option for addressing the polarization purity is rigorous prelaunch antenna characterization, which can be used for postprocessing correction. An extensive combination of measurements and analyses verified the antenna performance, which is summarized in Table V [15].

The performance requirements of the antenna system are based on the simulation described previously. To reduce the contamination from sidelobes, the antenna efficiency goal is 95% for all frequencies. The polarization purity is quantified in terms of the maximum coupling (control requirement) and residual coupling (knowledge requirement) for the various bands. The polarization purity control requirement is 99%, which corresponds to an allowable cross polarization of -20 dB. The polarization purity knowledge requirement is 99.9% for the polarimetric bands, and 99.5% for the vertical and horizontal bands. This results in residual cross-polarization coupling of -30 and -23 dB for the polarimetric and linear bands, respectively.

The most challenging aspect of the antenna subsystem is the characterization of the beam parameters. A polarimetric microwave radiometer measures the Stokes parameters, which, as described above, quantify the polarization properties of the emitted energy from a scene. Therefore, it is important to minimize and characterize the cross polarization in the antenna and OMT. The relationship between the scene brightness temperature, T_{B} and the brightness temperatures entering the radiometer receivers, T_A, can be described by the following equation, where M^{-1} represents the inverse Stokes Coupling Matrix. Prelaunch characterization provides the knowledge of M^{-1}, which is used to calculate T_{B}

$$\overline{T}_{\mathrm{B}} = \overline{\overline{M}}^{-1}\overline{T}_A.$$

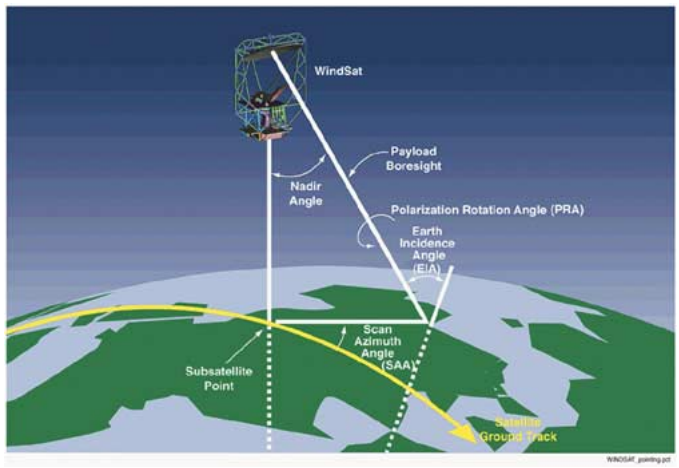

Fig. 5. Definition of WindSat geometry and pointing angles.

In addition to polarization coupling due to the antenna structure, coupling occurs when the spacecraft polarization basis is rotated with respect to the earth surface polarization basis. This form of coupling can be corrected by a matrix multiplication [12], which relieves the alignment requirement, but there remains a knowledge requirement of the polarization rotation angle (PRA) of 0.05° or less for both the bias and random components. To maintain the linearity of brightness temperature with EIA variation, the maximum allowable variation will be 0.25°, with a knowledge requirement of 0.05°. The various angles referenced are depicted in Fig. 5.

In order for the antenna measurements and pointing calculations to be valid, the antenna system alignments must be characterized and maintained. Therefore, the WindSat integration and test program included a rigorous alignment measurement campaign. The layout and alignment of the antenna system was mapped at the antenna range during the antenna pattern calibration. Additional alignment and pointing measurements were measured following shipping, thermal, and vibration testing. This process confirmed that the antenna system as characterized on the antenna range was unchanged at launch.

The on-orbit calibration is similar to that of heritage sensors. Once per scan, the feedhorns pass beneath a stationary warm calibration target and cold sky reflector, providing regular in-flight calibration of the instrument. Because of the differences in horn aperture size with respect to the warm load and

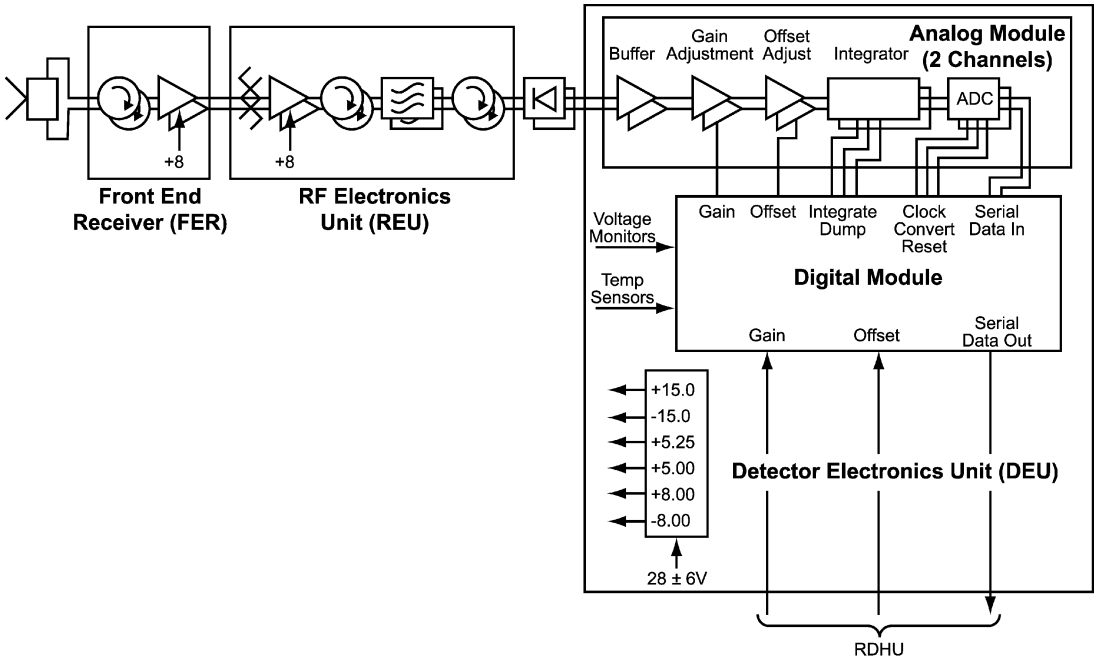

Fig. 6. WindSat receiver architecture for a polarization pair.

the cold sky reflector, the number of samples of each calibration target is different for each frequency, with the minimum number occurring for the 6.8-GHz channel (six samples of the warm load and two samples of the cold load). All calibration data are downlinked directly, with no onboard processing.

The warm load is a well-matched broadband microwave load composed of tapered pyramids coated with a 2.29-mm layer of Eccosorb CR-117 Epoxy (a microwave absorbing material). The calibration target has a teardrop shape to optimize the number of samples while minimizing scan occlusion and has a 7.62-cm shroud to ensure excellent coupling and minimize thermal gradients across the load. The warm load is passively heated through exposure to the radiator panels on the top deck of the WindSat canister. Six platinum resistance thermometers (PRT) mounted in the aluminum base of the warm load measure the warm load temperature.

The cold sky reflector (CSR), like the main reflector, is fabricated of graphite epoxy coated with at least 3.27μm of VDA and a protective layer of silicon oxide. The surface tolerance is 127μm. The CSR is sized so that when a feed horn passes under it, no part of the feed pattern sees the main reflector. In addition, the CSR was designed to receive less than 0.15 K of radiation from the earth.

B. Receiver Subsystem

The receiver subsystem accepts the energy from the 11 feed horns and provides amplification and filtering, producing 22 discrete digital signals channels to the data handling system. Fig. 6 depicts the receiver architecture. All of the channels are implemented as direct detection receivers. The nonlinearity of the receiver is driven by the detector diode and is less than 0.1%. The receiver dynamic range accommodates input antenna temperature ranging from 3–330 K as well as internal gain changes due to temperature and aging. The receiver subsystem is subdivided into three units; the front-end receiver (FER),which performs matching and low-noise amplification; the receiver electronics unit (REU) providing additional gain and filtering; and the detector electronics unit (DEU), which performs integration, detection, A/D conversion, gain and offset adjustment. Each channel is integrated and sampled to achieve spatial Nyquist sampling along scan. The 37-GHz channels, which have the smallest 3-dB beamwidth, are integrated for 1.08 ms, while the 6.8-GHz channels, which have the largest 3-dB beamwidth, are integrated for 5.0 ms. The integration times can be reprogrammed on orbit.

As stated earlier, taking the difference between polarization pairs ($\pm 45^\circ$ and LC/RC) produces the third and fourth Stokes parameters. In the process, common mode calibration errors are minimized because the absolute brightness differences are small. However, receiver nonlinearity does not cancel and can result in a significant calibration error. The nonlinearity of a radiometer receiver results from amplifier saturation and detector nonsquare-law response, of which the latter is dominant. Regardless of the cause, both types of distortion have an effect on the radiometric performance. Amplifiers were selected to form pairs with nearly identical measured performance and attenuators were used to optimize the final receiver gains. Following the suggestion of Hoer *et al.* [16], we optimized the linearity of the diode detectors by adjusting the load resistance, again in pairs so that performance could be matched. The linearity of the receivers was tested using the two-tone method [17] over the thermal operating range. Nonlinearity was measured to be less than 0.1% and typically 0.06%. As an additional test, the receivers were tested in the thermal vacuum chamber using precision cold and variable targets in addition to the WindSat flight warm load. The U.K. Meteorological Office Remote Sensing Instrumentation (U.K. Met Office RSI) group developed the cold and variable calibration target system. The radiometer temperature was cycled over its operating range and performance tested at 0 °C, 20 °C, and 40 °C. At each system temperature plateau the variable target temperature was stepped from 85 K to 325 K

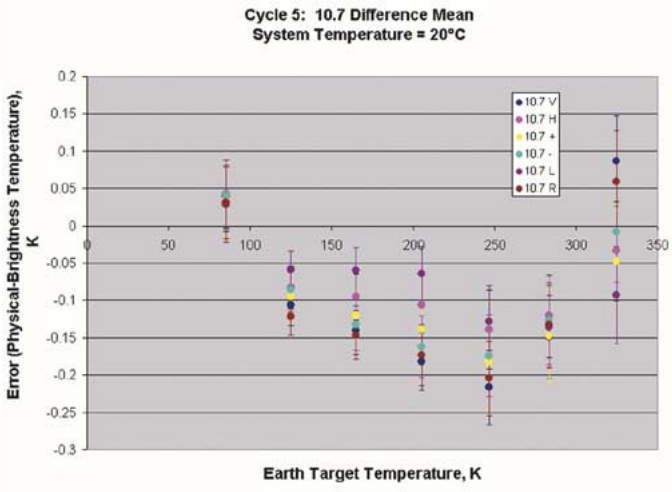

Fig. 7. Absolute accuracy nonlinearity effects measured in thermal vacuum for 37 GHz at system temperature of 20 °C. Data are variable target brightness calibrated with space target (82 K) and WindSat warm load (283 K). Displayed errors include calibration target errors.

in 40-K increments, while the cold target was maintained at approximately 85 K. From this dataset, a number of key performance parameters were examined, including receiver linearity. For each of the three polarimetric frequencies, we calculated the difference between the variable target temperature and the brightness temperature measured by WindSat. These results, at the nominal system operating temperature of 20 °C, are presented in Fig. 7. They exhibit the typical U-shape curve for nonlinearity effects on a two-point calibration. Channel pair differences are typically less than 0.1 K.

C. Thermal and Structural Subsystem

The WindSat structure is significantly larger than it predecessor, the SSM/I. The structure stands 3.20 m tall, 2.52 m wide, and 2.52 m deep. The antenna support structure consists of graphite reinforced epoxy composite tubes, which provide the needed stiffness and low mass. The remainder of both the stationary and spinning structures are built from aluminum honeycomb.

The WindSat thermal subsystem was designed to handle a number of difficult requirements driven by the operating temperatures of the electronics, the pointing and polarization purity requirements of the antenna, and the thermal stability and uniformity of the warm calibration target.

The receivers, data handling units, and low-noise amplifiers (LNAs) (attached directly to the feed horns) must be maintained within the operating temperature range of 0 °C to 40 °C. The warm load does not have a specific required temperature. It is desired to maintain the warm load between 250–330 K to span the scene temperatures and stay within the dynamic range of the receivers. The design also ensures that horizontal gradients across the warm load shall be less than 0.4 K. The rate of change of the temperatures of the receiver components was also specified at less than 0.01 °C/scan to minimize short-term gain instability. For longer-term thermal stability, the WindSat system is designed to maintain its temperature to within ± 1.0 °C/orbit. Features of the thermal design include survival heaters to maintain the integrity of the payload under nonnormal operating conditions and heat pipes on the top deck to dissipate heat from the electronics and provide passive, steady-state heat for the warm calibration target. Copper-water heat pipes in the feedbench transfer heat from the LNAs to the feedbench radiator.

D. Data Handling

The Data Handling System (DHS) creates the WindSat data stream and performs various command and control functions. The DHS comprises two subsystems: the Rotating Data Handling Unit (RDHU) and the Stationary Data Handling Unit (SDHU). The RDHU receives digital data from the five DEUs and deletes data collected while the feeds are partially occluded by the cold sky reflector. Together, the two units of the DHS generate the integrator sampling signal and synchronize sampling with the antenna scan to maximize calibration repeatability. The DHS provides command and telemetry interfaces for the GPS receiver, Bearing and Power Transfer Assembly (BAPTA) electronics, momentum wheel assembly, and launch locks. A single real-time mission data stream for all payload data sources and supporting telemetry is produced in the DHS for direct tactical downlink of data. The telemetry data list includes radiometer data, warm load PRT measurements, time tag data, GPS position, velocity and time data, low-precision temperature data (main and cold reflectors, struts, feed, OMT, feedbench, receiver, DHS, BAPTA drive bearings, and decks), and BAPTA and momentum wheel motor currents and spacecraft attitude data. The attitude data are collected by the Coriolis spacecraft and passed to the WindSat DHS to be incorporated into the mission data stream.

IV. Ground Data Processing Software

The WindSat payload produces approximately 200 MB of data per orbit, or 3.0 GB/day. NRL has developed Ground Data Processing Software (GDPS) to process 100% of available downlink data, providing accurate and precise data products as dictated by the WindSat mission requirements. The GDPS is also designed to satisfy the data latency requirement of 24-h turnaround in the first year and 4-h turn-around in the second and third years of the mission. The GDPS must also be portable to the operational Navy for use following WindSat calibration and validation.

The GDPS comprises four main processors: the Raw Data Record Processor (RDRP), the Temperature Data Record Processor (TDRP), the Sensor Data Record (SDRP), and the Environmental Data Record Processor (RDRP). The flow diagram for these functions is shown in Fig. 8.

The RDRP receives the WindSat data stream, including receiver, calibration, housekeeping, and spacecraft attitude data. The RDRP decodes, unpacks, reformats and merges these data in preparation for the remaining data processing steps.

The TDRP receives the formatted data and performs the first four critical functions. First, the TDRP calibrates the raw counts into radiances using the calibration target measurements and the sensor calibration constants file. Then, each channel is geolocated using the scan angle, spacecraft attitude and ephemeris, and the antenna pointing offsets. A surface type (e.g., land, ocean, coastline, etc.) is then identified for each footprint from a static surface database. Using the spacecraft

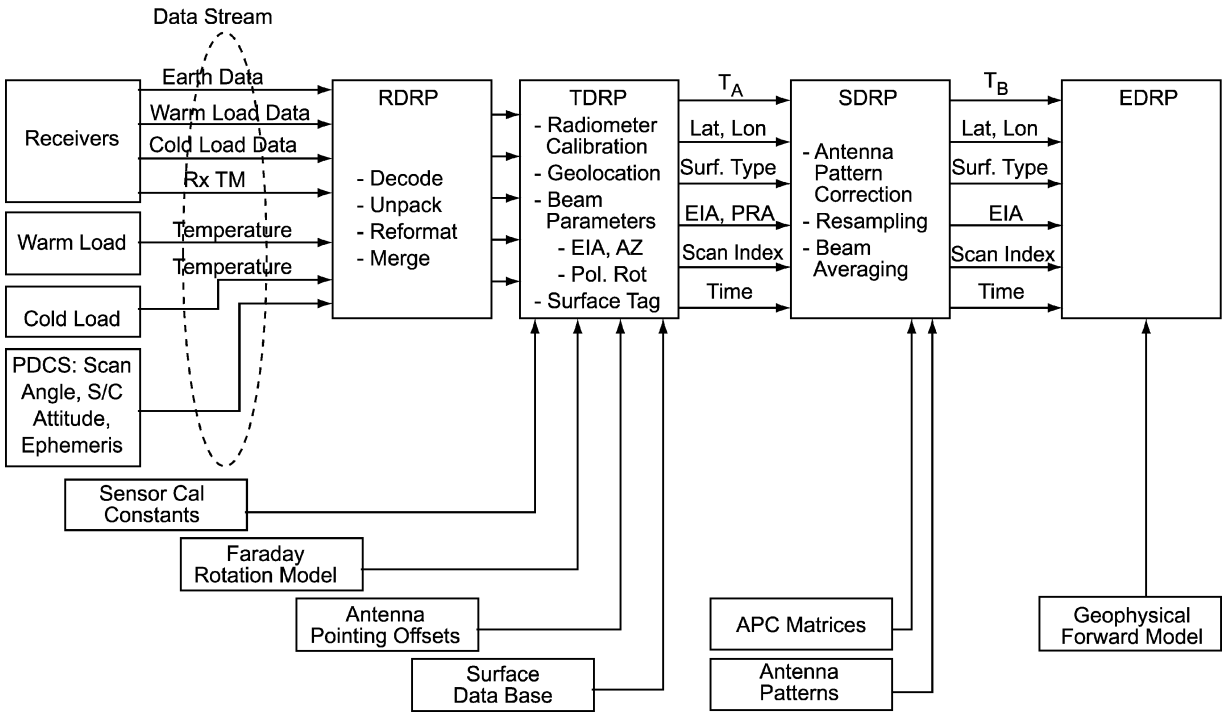

Fig. 8. Top-level diagram of WindSat ground data processing system.

ephemeris and an ionosphere model, the Faraday rotation is calculated. The Faraday rotation angle and the spacecraft attitude and ephemeris are then used to calculate various antenna parameters, such as the EIA, the PRA, and the surface compass azimuth angle (CAA), which describes the sensor look direction on the surface.

The next level of processing occurs in the SDRP, which screens the TDR data for anomalies such as RFI and rain cells, and forms the third and fourth Stokes parameters by taking the difference of the appropriate polarizations. The antenna pattern correction (APC) follows, using stored cross-coupling correction matrices (M^{-1}) and feed spillover efficiencies. Because each frequency set has a different beamwidth and relative pointing, the final stage of the SDRP resamples and averages the beams to yield collocated pixels at a common resolution. This is the highest level of phase 1 (brightness temperature) processing before the EDRP.

The EDRP provides the WindSat Level 2 processing. The inputs to the EDRP are the calibrated, geolocated, coregistered WindSat Stokes parameters at 10.7, 18.7, and 37 GHz, and the vertical and horizontally polarized brightness temperatures at 6.8 and 23.8 GHz. These sets of 16 quantities form the basic measurement vector for the retrieval. The quantities that are retrieved from this set of measurements include ocean surface wind speed and direction, as well as SST and atmospheric parameters such a precipitable water vapor, rain rate, and cloud liquid water.

V. Early Orbit System Performance

After being powered on on January 24, 2003, the WindSat radiometer achieved thermal stability in less than 36 h, at which time the receiver gains also stabilized. The gains and receiver

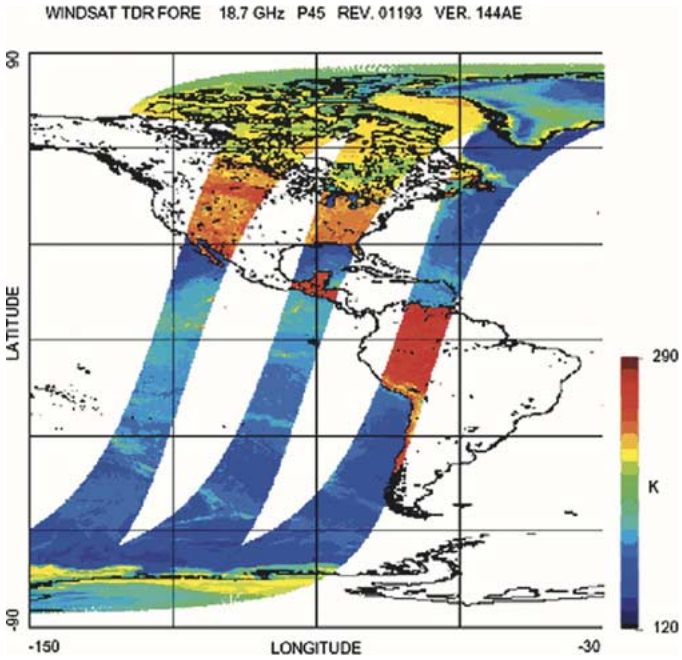

Fig. 9. WindSat image showing three consecutive descending passes of 18.7-GHz $+45^\circ$ (18P) channel.

offsets were adjusted via ground commands to optimize the dynamic range of the receivers. The WindSat calibration and validation (cal/val) team then began rigorous analysis of the system performance and debugging of the GDPS. One of the first products from this process was radiometric imagery for all 22 channels. As an example, Fig. 9 shows a TDR image of three consecutive descending passes for the 18.7-GHz $+45^\circ$ polarization channel collected on March 31, 2003. Several features stand out in the false-color image. The visible structures of

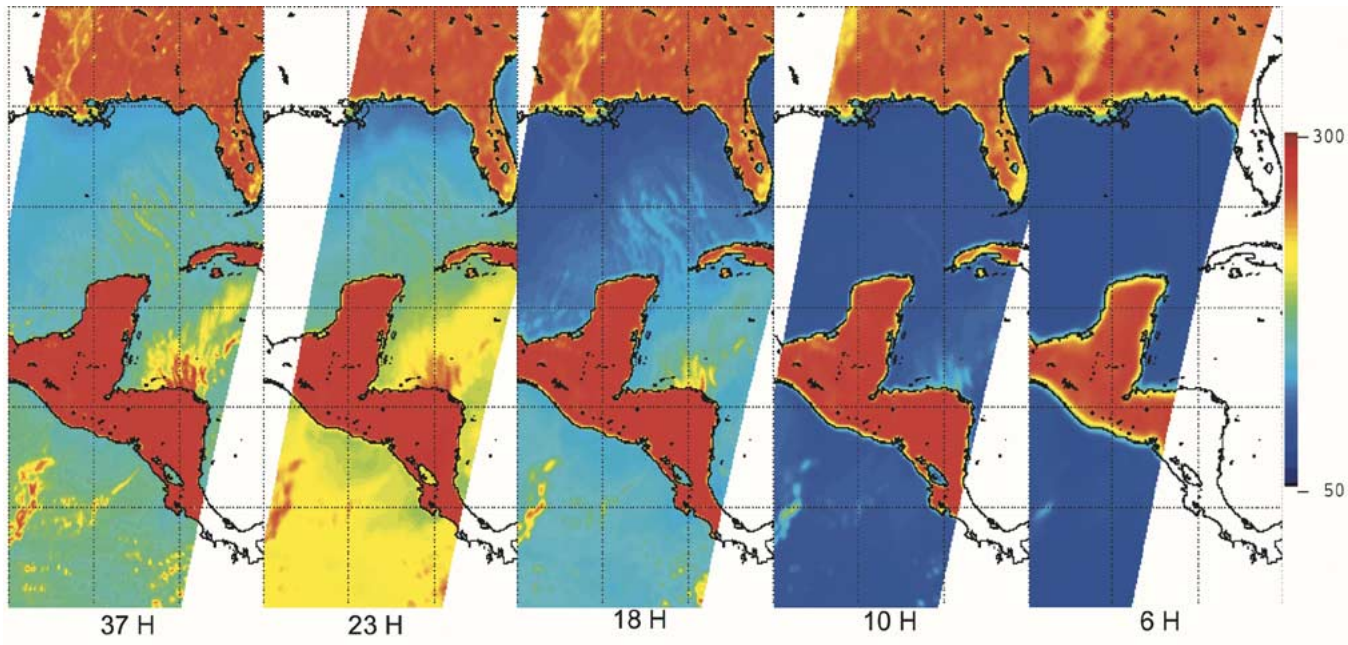

Fig. 10. Composite image showing horizontal polarization at each of five WindSat frequency bands. Area is Yucatan peninsula of Mexico.

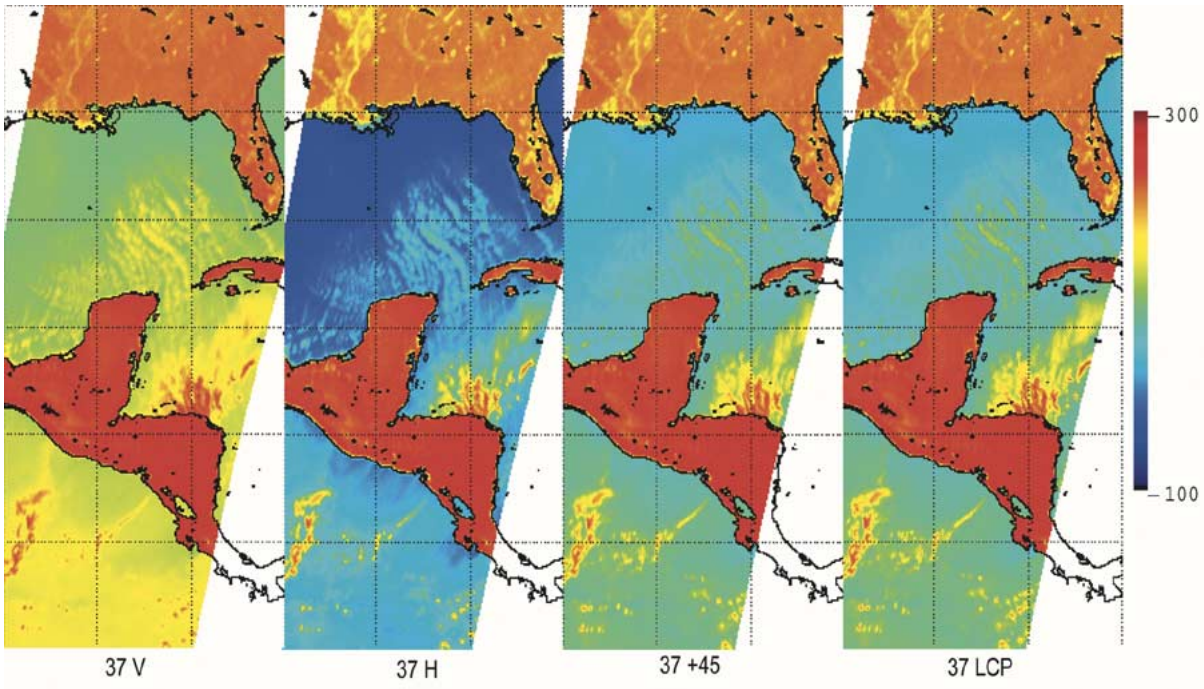

Fig. 11. Composite image showing 37-GHz brightness temperatures at vertical, horizontal, +45, and left-circular polarizations.

bright bands and other regions of locally high brightness temperatures over the ocean are typical of atmospheric variations in water vapor, clouds and rain. In the North Atlantic, the brightness temperatures in the Labrador Sea and Hudson Bay (colored yellow/green in the image) are higher than the ambient ocean and are typical of sea ice signatures, whereas the cooler brightness temperatures over Greenland are representative of a permanent ice sheet. Over land, there are also noticeable differences in brightness temperatures, which are due to differences in the physical temperature of the terrain, such as between North America (early spring) and equatorial South America. Last, in North America, the brightness temperature decreases with increasing latitude over northern Canada, which is consistent with signatures of snow cover in those regions for this time of year.

Fig. 10 highlights a portion of this same pass over Mexico and Central America, showing simultaneous images at horizontal polarization for each of the five WindSat frequencies. In this series of images, one can see how the various frequencies respond differently to the same oceanic and atmospheric conditions, most noticeably in the increased sensitivity to clouds and water vapor (which appear as bright features) in the higher frequency channels. One can also see differences in swath width resulting from the feedbench layout. To illustrate the differences among polarizations at the same frequency, Fig. 11 depicts the 37-GHz imagery at vertical, horizontal, $+45^{\circ}$ linear, and

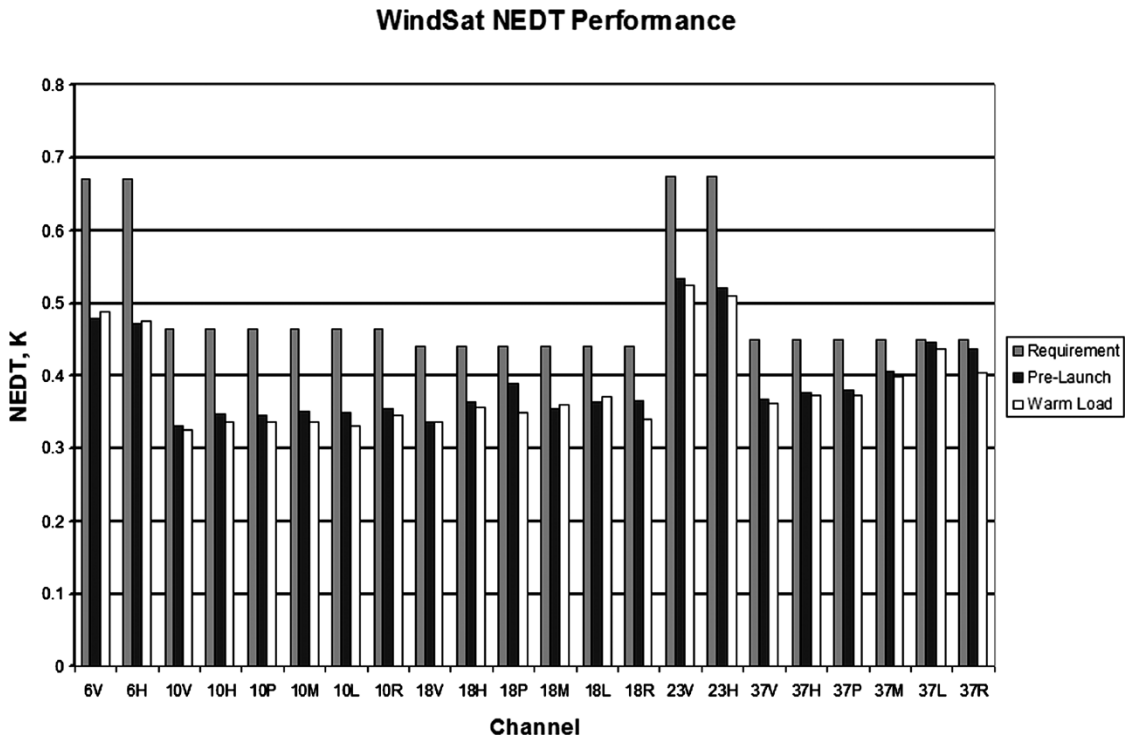

Fig. 12. WindSat receiver NEDT performance. Plot shows requirement, prelaunch test, and on-orbit performance while viewing warm load. Requirement and prelaunch data normalized to on-orbit warm load temperature of 283 K.

left-circular polarizations. (For these color scales, differences between left and right circular polarizations are too subtle to be instructive; the same is true for $+45^\circ$ and -45° linear polarizations, so only one of each pair is shown here.) When comparing these images, it is clear that over the ocean the magnitudes of $+45^\circ$ and left-circular brightness temperatures lie between the values of the vertical and horizontal polarizations, as is expected for ocean scenes viewed in the WindSat geometry.

Images such as these contain a great deal of information and serve as a qualitative assessment of WindSat performance. The rest of this paper will focus on quantitative results from the early system performance assessment.

A. Receiver Noise Performance

The noise equivalent differential temperature (NEDT) is a measure of the sensitivity of the measured brightness temperature to changes in the scene brightness. For a single sample from a total power radiometer, we use (2) to calculate system NEDT as a function of the system parameters [18].

$$\mathrm{NEDT} = T_{\mathrm{sys}} \sqrt{\frac{1}{B\tau} + \left(\frac{\Delta G}{G}\right)^2} \tag{2}$$

where

$T_{\mathrm{sys}} = T_{\mathrm{Noise}} + T_{\mathrm{Antenna}}$ system noise temperature + scene-dependent input to antenna;

B channel predetection bandwidth (design parameter);

τ channel postdetection integration time (design parameter);

G channel gain (design parameter);

ΔG channel gain fluctuation over integration time (LNA device property).

The noise temperature and gain fluctuation terms generally increase as the physical temperature of the receiver chain increases. The WindSat NEDT requirements were derived from retrieval sensitivity studies during the first phase of the program. The NEDT for each radiometer was measured at various stages of the program, with the final prelaunch measurements occurring during thermal/vacuum testing. Postlaunch early-orbit NEDT estimates have been made based on samples from the warm calibration target and the cold space reflector view. In Fig. 12, we compare the NEDT requirement with the pre- and postlaunch measurements of NEDT. For this comparison the NEDT requirement was normalized to the conditions under which the pre- and postlaunch measurements were made: receiver physical temperature of 24 °C and antenna scene temperature of approximately 283 K. The postlaunch numbers are based on the warm calibration target, which is presents an upper bound on the NEDT. The performance for all channels meets or exceeds the requirements. This analysis was completed shortly after WindSat became thermally stable, in February 2003.

B. Gain Stability

WindSat is calibrated once in each scan period of 1.9 s, so the minimum gain stability requirement is that the gain should not fluctuate over this period. WindSat contains no automatic or stepped gain control, but rather the gain is allowed to drift freely. The rate of gain change was managed through a passive

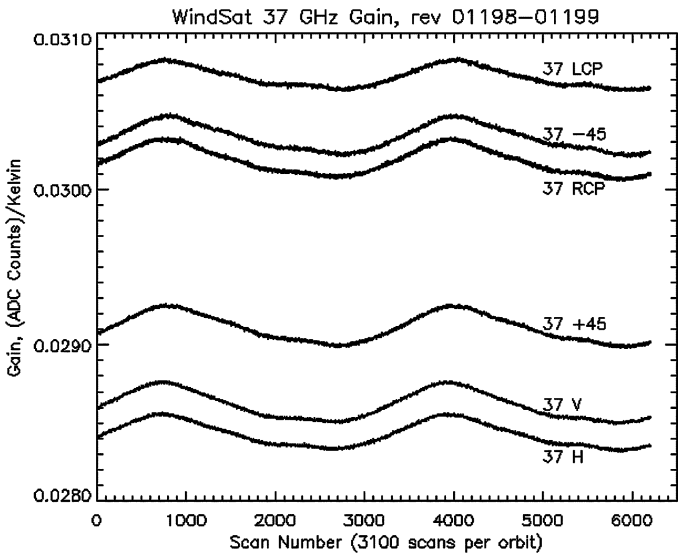

Fig. 13. Gain of WindSat 37-GHz channels over two orbits. Drifts track orbit induced thermal variations.

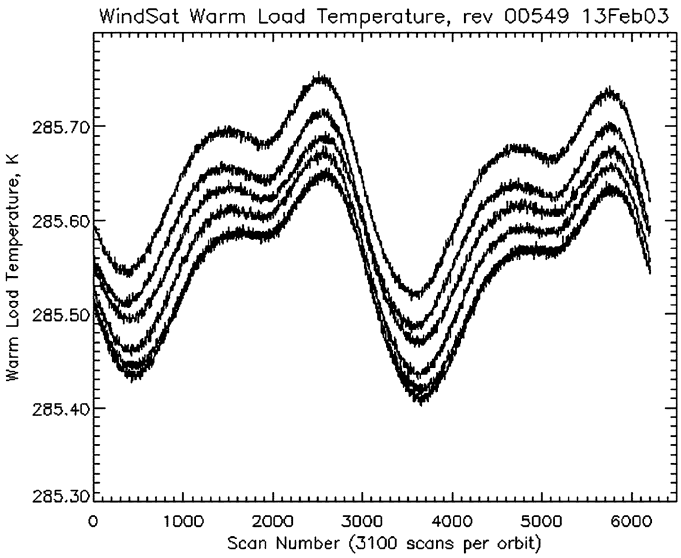

Fig. 15. WindSat warm load physical temperature over two orbits. Variations are due to orbital variations in thermal system.

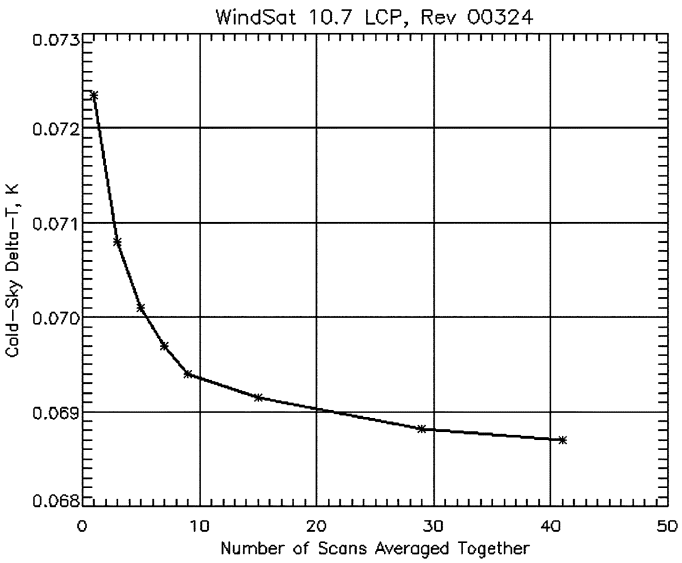

Fig. 14. WindSat calibration NEDT as a function of number of scans of calibration data averaged together. Gain instability eventually causes NEDT to increase with increasing number of scans. WindSat gains are sufficiently stable that calibration data more than 40 scans may be averaged.

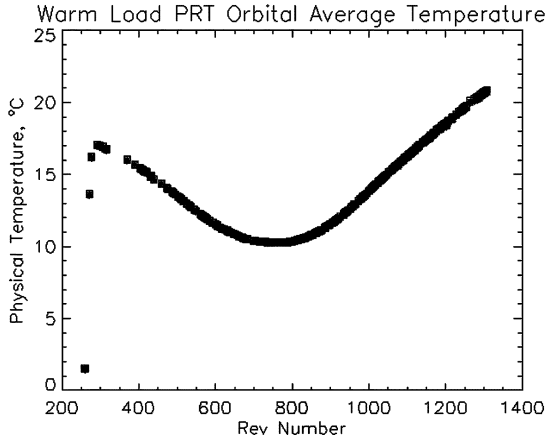

Fig. 16. WindSat warm load physical temperature over approximately 1000 orbits or about 70 days. Each point represents orbital average for single thermistor.

thermal design. In orbit, the gain varies sinusoidally through the orbit cycle, as shown in Fig. 13. The gain is calculated using

$$G = \frac{\overline{V}_{\text{warm}} - \overline{V}_{\text{cold}}}{\overline{T}_{P,\text{warm}} - \overline{T}_{P,\text{cold}}}.$$

The voltages in the numerator V_{warm} and V_{cold} are averages of the radiometric samples across the warm and cold targets. Averaging samples across multiple scans reduces the impact of noise on these measurements. The receiver gain is sufficiently stable to allow averaging for as many as 40 scans (approximately 80 s); however, the bulk of the improvement is achieved after averaging calibration samples over 15 scans. The measured improvement in the NEDT of the calibration samples due to averaging over multiple scans is shown in Fig. 14.

C. Nominal Calibration Target Stability

During the early orbit period we carefully monitored the short-term stability of the warm calibration target. Temperature measurements from one of the embedded PRTs over a two-orbit period are presented in Fig. 15. The nominal peak-to-peak variation is less than 1 K, with a maximum observed rate of change of 0.0006 °C/s. The nominal thermal gradient across the target is less than 0.1 K. Fig. 16 shows the orbitally averaged temperature as measured by each of the six PRTs on the warm load over the first 90 days (February–April 2003). This slow fluctuation is consistent with the seasonal changes in the sun beta angle. The short eclipse season, centered on the northern hemisphere summer solstice, is expected to be the most thermally stressing for the WindSat system and calibration target. We will continue to closely monitor the thermal performance throughout this time period.

The cold space reflector provides the cold calibration point for the gain calculation. The cold space reflector has an extremely low emissivity and completely occludes the feed horn

view of the main reflector when the feeds pass underneath it. There is no instrument or spacecraft structure near the beam, which provides a stable cold point for each of the channels. There are no detectable changes in the cold space reflector performance with temperature. Additional analysis and on-orbit performance evaluation is currently underway.

D. Spin Rate Stability

WindSat spins at a rate of 31.595 r/min, or once every 1.8990 s. The variation since the instrument stabilized is ± 0.005 r/min or 0.0003 s per revolution. This translates to an antenna boresight variation of $\pm 0.057^\circ$, or less than a 1-km pixel position error when projected to the earth's surface.

VI. Swath Definition

The WindSat feedhorn layout was described in Section III. The position and pointing of each horn relative to the main reflector determines its unique, unobstructed swath. The intersection of the 11 individual swaths is identified as the WindSat common fore and aft swaths. The WindSat swath requirement was simply to maximize swath width while maintaining a two-look (fore/aft) capability. The swath was analyzed for each channel using orbitally averaged data, and regions showing evidence of partial occlusion by the calibration loads were identified. While some frequency bands have a swath width greater than 1200 km in the forward look direction, the common swath width is approximately 950 km (68° of scan angle); the aft common swath is 350 km (23° of scan angle). The aft common swath does not contain 6.8-GHz data, for which the aft swath does not intersect the other channels due to the position of that feed on the edge of the feedhorn layout. More rigorous analysis of the along-swath stability and any swath edge bias is currently underway. As the analysis of the channel performance across swath progresses, these nominal common swaths may change slightly.

VII. Geolocation

The wind direction will be derived from very small differences in polarization pairs. Therefore, pointing errors have a large impact on the validity of the derived wind vectors, primarily because of the impact of earth incidence angle variations on the brightness temperature and polarization rotation angle variations on the cross-polarization coupling. Accordingly, Coriolis/Windsat was designed to provide knowledge errors of $\pm 0.05^\circ$ bias and $\pm 0.05^\circ$ random components in each EIA and PRA. These requirements equate to ± 1 km of geolocation error on the earth-projected beams. One should note that the geolocation requirement is 4 km, but that the pointing requirements result in better than required geolocation.

A geolocation analysis performed during the early orbit period compared WindSat imagery for each channel with high accuracy coastline maps. The land–water transition produces a sharp change in the WindSat data, because water is radiometrically colder than land. The rate of brightness temperature change was calculated along a track crossing an ocean–land boundary. The position of maximum rate of change was identified as the WindSat-derived coastline, which could then be compared with a global coastline database. Fig. 17 shows an

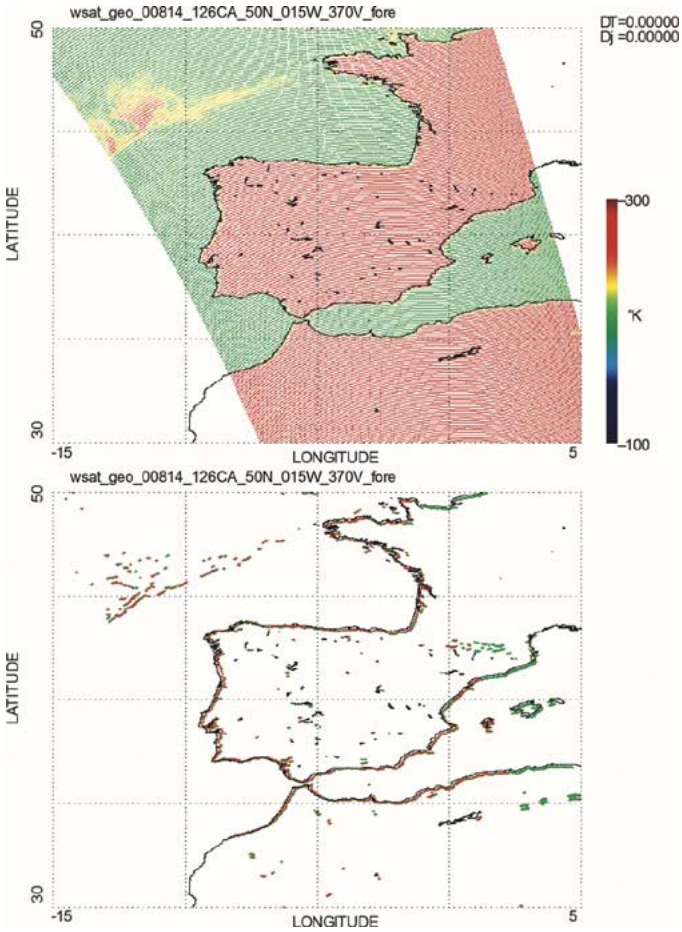

Fig. 17. WindSat geolocation analysis results. Upper shows WindSat brightness temperatures over Spain. Lower image highlights WindSat detected coastline by plotting points of maximum brightness rate of change.

example of this analysis. Errors on the order of 10 km were identified and traced to two timing issues. The dominant error was driven an inaccurate time assignment error on the GPS data. The assignment was in error by 1 s, which appeared as a positional offset in the WindSat data. The impact of this error was compounded by the fact that the attitude data used by the ground processing software to make attitude corrections to the brightness temperatures were not coincident with the WindSat measurements. A second type of error appeared as an accumulating 5 μs per sample radiometer time assignment error along the scan. This error was reset to zero at the time synch for each scan. This error was traced to a miscalculation in the number of clock cycles required to acquire and store each sample.

Corrections for each of these timing errors bring the geolocation error down to less than 5 km. At the time of this writing, further in-depth analysis is ongoing to identify and correct the residual geolocation and pointing errors.

VIII. CAL/VAL Purpose and Importance

Prior to public release of data products, the WindSat system must go through the calibration and validation process, which has two primary purposes. The first is to verify the WindSat radiometer absolute accuracy as driven by the calibration target accuracy and knowledge, the receiver performance, the antenna characterization and antenna pattern correction (APC), and the

geolocation and pointing processing. The second purpose is to validate the sea surface wind speed and direction environmental data products. A key part of this process is to identify and quantify error sources and, if necessary, generate new sensor calibration coefficients, algorithms, and environmental data record (EDR) retrievals to bring the data products into specification.

The WindSat system presents several unique calibration and validation challenges. The wind direction signal, which is a sinusoidal signal as a function of wind direction (relative to the look direction of the sensor) is two orders of magnitude smaller than the vertical and horizontal polarizations typically measured by passive microwave imagers. As such, the design sensitivity analysis resulted in sensor noise and absolute accuracy requirements approximately 50% tighter than the current SSM/I operational performance. Antenna and receiver polarization purity and horn/antenna/payload alignments are significant elements of the accuracy error budget.

The results of the first SSM/I (F-8) cal/val clearly demonstrate the importance of a comprehensive cal/val program [1], [2]. Through the efforts of an NRL-led team composed of government and university microwave remote sensing experts led by NRL, the SSM/I validation team demonstrated that many of the retrieval algorithms that failed to meet specification could be brought into compliance with postlaunch tuning and quality flags. The WindSat cal/val plan is largely modeled on the successful SSM/I cal/val plan and lessons learned from the process.

Finally, WindSat is tasked with demonstrating the capability of polarimetric microwave radiometry to measure the ocean surface wind direction from space. Therefore, it is critical that all sensor errors be understood and separated from phenomenology of the wind direction signal.

IX. Conclusion

The WindSat polarimetric microwave radiometer was launched on the Coriolis mission on January 6, 2003. The objective of the WindSat program is to demonstrate the viability of polarimetric microwave radiometry to measure the ocean surface wind vector. The system was designed, built, integrated, and tested in response to the requirements of the U.S. Navy and the NPOESS Integrated Program Office.

Following launch, the WindSat team has been analyzing the WindSat data and conducting the calibration/validation. To date the instrument has been performing extremely well. Gain stability and NEDT levels are much better than required specifications. Geolocation errors are well within the smallest antenna beam size, while pointing performance continues to be analyzed.

The ultimate objective of the WindSat mission is to demonstrate the capability of polarimetric radiometry to retrieve the ocean surface wind vector. The early performance of WindSat gives us confidence that the Stokes parameter data will be of enough quality to facilitate this demonstration. The work of retrieving the wind vector is ongoing.

Acknowledgment

The authors wish to acknowledge the talents and efforts of the Naval Research Laboratory Naval Center for Space Technology, whose engineers built, tested, and operate WindSat.

References

[1] J. P. Hollinger, Ed., "DMSP Special Sensor Microwave Imager Calibration/Validation," Nav. Res. Lab., Washington, DC, NRL Final Rep., vol. I, June 1989.

[2] J. P. Hollinger, J. L. Peirce, and G. A. Poe, "SSM/I instrument evaluation," *IEEE Trans. Geosci. Remote Sensing*, vol. 28, pp. 781–790, Sept. 1990.

[3] M. A. Goodberlet, C. T. Swift, and J. C. Wilkerson, "Ocean surface wind speed measurements of the Special Sensor Microwave/Imager (SSM/I)," *IEEE Trans. Geosci. Remote Sensing*, vol. 28, pp. 823–828, Sept. 1990.

[4] F. J. Wentz, "Measurement of oceanic wind vector using satellite microwave radiometers," *IEEE Trans. Geosci. Remote Sensing*, vol. 30, pp. 960–972, Sept. 1992.

[5] P. S. Chang and L. Li, "Ocean surface wind speed and direction retrievals from the SSM/I," *IEEE Trans. Geosci. Remote Sensing*, vol. 36, pp. 1866–1871, Nov. 1998.

[6] S. H. Yueh, W. J. Wilson, F. K. Li, W. B. Ricketts, and S. V. Nghiem, "Polarimetric brightness temperatures of sea surfaces measured with aircraft K- and Ka-band radiometers," *IEEE Trans. Geosci. Remote Sensing*, vol. 33, pp. 1177–1187, Sept. 1997.

[7] S. H. Yueh, W. J. Wilson, S. J. DiNardo, and F. K. Li, "Polarimetric microwave brightness signatures of ocean wind direction," *IEEE Trans. Geosci. Remote Sensing*, vol. 37, pp. 949–959, Mar. 1999.

[8] P. S. Chang, P. W. Gaiser, L. Li, and K. M. St. Germain, "Multi-frequency polarimetric microwave ocean wind direction retrievals," in *Proc. IGARSS*, Singapore, 1997.

[9] J. R. Piepmeier and A. J. Gasiewski, "High-resolution passive polarimetric microwave mapping of the ocean surface wind vector fields," *IEEE Trans. Geosci. Remote Sensing*, vol. 39, pp. 606–622, Mar. 2001.

[10] G. A. Wick, J. J. Bates, and C. C. Gottschall, "Observational evidence of a wind direction signal in SSM/I passive microwave data," *IEEE Trans. Geosci. Remote Sensing*, vol. 38, pp. 823–837, Mar. 2000.

[11] K. M. St. Germain, G. A. Poe, and P. W. Gaiser, "Polarimetric emission model of the sea at microwave frequencies and comparison with measurements," *Progr. Electromagn. Res.*, vol. 37, pp. 2–32, 2002.

[12] L. Tsang, J. A. Kong, and R. T. Shin, *Theory of Microwave Remote Sensing*. New York: Wiley, 1985.

[13] P. W. Gaiser, G. A. Poe, and K. M. St. Germain, "Critical design issues for space borne polarimetric radiometry," in *Proc. IGARSS*, Seattle, WA, 1998.

[14] A. J. Simmons, "Phase shift by periodic loading of waveguide and its application to broad-band circular polarization," *IRE Trans. Microwave Theory Tech.*, vol. 3, no. 6, pp. 18–21, 1955.

[15] W. L. Lippincott, T. A. Gutwein, H. E. Bartlett, M. Smythers, P. W. Gaiser, and W. J. Purdy, "Antenna design, modeling and testing on the WindSat wind direction measurement system," Nav. Res. Lab., Washington, DC, NRL Tech. Memo. Rep., Mar. 2002.

[16] C. A. Hoer, K. C. Roe, and C. M. Allred, "Measuring and minimizing diode detector nonlinearity," *IEEE Trans. Instrum. Meas.*, vol. IM-25, pp. 324–329, Dec. 1976.

[17] V. S. Reinhardt, Y. C. Shih, P. A. Toth, S. C. Reynolds, and A. L. Berman, "Methods for measuring the power linearity of microwave detectors for radiometric applications," *IEEE Trans. Microwave Theory Tech.*, vol. 43, pp. 715–720, Apr. 1995.

[18] F. T. Ulaby, R. K. Moore, and A. K. Fung, *Microwave Remote Sensing*. Reading, MA: Addison-Wesley, 1981, vol. I.

Peter W. Gaiser (S'91–M'93–SM'04) received the B.S. degrees in electrical engineering from Virginia Polytechnic Institute and State University, Blacksburg, in 1987, and the Ph.D. degree from the University of Massachusetts, Amherst, in 1993, where he studied microwave remote sensing, with emphasis on synthetic aperture interferometric radiometry.

He has been with the Naval Research Laboratory (NRL), Washington, DC, since 1993, and currently heads the Microwave Remote Sensing Section, Remote Sensing Division at NRL. While at NRL, he has been involved in polarimetric radiometry research. His research interests also include instrument design, data collection, and model development specifically for the purpose of ocean wind vector measurements from space. He is the Principal Investigator for the WindSat spaceborne polarimetric microwave radiometer demonstration project.

Karen M. St. Germain (S'88–M'91–SM'03) received the B.S. degree in electrical engineering from Union College, Schenectady, NY, in 1987, and the Ph.D. degree from the University of Massachusetts, Amherst, in 1993.

From 1987 to 1993, she was a Research Assistant in the Microwave Remote Sensing Laboratory, University of Massachusetts, where her doctoral research focused on passive microwave remote sensing of oceans and ice. In 1993, she joined the Faculty of the Department of Electrical Engineering, University of Nebraska, Lincoln. While at the University of Nebraska, she taught courses in electromagnetics, signal processing, and radar system design, and expanded her research interests to include passive and active remote sensing of vegetation and soil moisture. In 1996, she left the University of Nebraska to take a position at the Naval Research Laboratory, Washington DC, where she is currently involved in remote sensing system development, spaceborne demonstration of remote sensing concepts, instrument calibration, radiative transfer theory, and algorithm development.

Dr. St. Germain has been a member of the IEEE Geoscience and Remote Sensing Society (GRSS) since 1988. She served as an Associate Editor of the IEEE GRSS Newsletter from 1994 to 1996 and was elected to the GRSS AdCom in 1997. She served as the Membership Chairman from 1997 to 1998 and has served as the Vice President for Meetings and Symposia from 1998 to 2003. She is currently Vice President of Operations and Finance. She was Co-Chairman of the Technical Program for IGARSS 2000 and is a member of Eta Kappa Nu and Tau Beta Pi. She currently serves on the U.S. National Research Council's Committee on Radio Frequencies (CORF).

Elizabeth M. Twarog received the B.S. degree from the University of Massachusetts, Amherst, in 1992, and the M.S. and Ph.D. degrees from Northeastern University, Boston, MA, in 1995 and 1998, respectively, both in electrical engineering.

From 1993 to 1998, she was a Graduate Assistant in the Radar Systems Laboratory, Northeastern University, in the field of polarimetric low-grazing angle radar sea scatter and airborne radar imaging of the coastal ocean. Since joining the Passive Microwave Section of the Naval Research Laboratory, Washington, DC, in 1999, she has been involved with microwave spaceborne polarimetric radiometry as a member of the WindSat technical and science teams.

Gene A. Poe (M'91) received the B.A. and M.S. degrees in electrical engineering from the University of California, Berkeley, in 1964 and 1965, respectively.

He has worked in wide-ranging companies responsible for the development of space-based passive microwave radiometer instruments (Aerojet Corporation: 1965–1972 and 1989–1993; Hughes Aircraft Company: 1976–1982). From 1986 to 1989 and from 1993 to the present, he has been with the Marine Meteorology Division, Naval Research Laboratory, Monterey, CA, working on microwave radiometric modeling and analysis of SSM/I data and the direct assimilation of microwave radiances for numerical weather prediction. He is currently Technical Leader for the joint Air Force/Navy DMSP calibration/validation effort of the Special Sensor Microwave Imager/Sounder.

Mr. Poe is a member of the American Mathematical Society.

William Purdy received the B.S. degree in mechanical engineering from the University of Maryland, College Park.

He has specialized in spacecraft systems engineering and spacecraft mechanisms over an 18-year career, including working at the Naval Research Laboratory from 1986 to 1999. He is currently the proprietor of Purdy Engineering from 1999 to the present. He has performed as a Systems Engineer on WindSat payload with responsibilities for alignments, antenna systems engineering, and mechanical systems engineering.

Donald Richardson received the B.S. and M.S. degrees from the University of Kentucky, Lexington, in 1978 and 1980, respectively.

He is currentaly a Software Developer and Scientist who has worked on several projects for NASA and the Naval Research Laboratory (NRL). For NASA, he has worked on data analysis and software development for the Upper Atmosphere Reseach Satellites' Halogen Occulation Experiment, the Cosmic Background Explorer, the Total Ozone Mapping Spectrometer, and Solar Backscatter Ultraviolet Spectrometer. In the late 1990s, he was the Vice President of Flytecomm of Florida, a small startup company developing software products to track in-flight aircraft based on a FAA data feed. For the past four years, he has been the Lead Programmer for NRL's WindSat and is responsible for the design and implementation of the processing code.

Walter Grossman (M'78), photograph and biography not available at the time of publication.

W. Linwood Jones (SM'75–F'99) received the Ph.D. degree in electrical engineering from the Virginia Polytechnic Institute and State University, Blacksburg, in 1971.

He is a Professor with the School of Electrical Engineering and Computer Science, University of Central Florida, Orlando. At UCF, he teaches undergraduate and graduate courses in communications, satellite remote sensing, and radar systems. He is also the Director of the Central Florida Remote Sensing Laboratory, where he performs research in satellite microwave remote sensing technology development. He is currently a member of the science teams for the Jet Propulsion Laboratory's SeaWinds Scatterometer Program and the NASA Goddard Space Flight Center's Tropical Rainfall Measuring Mission.

David Spencer received the B.S. and M.S. degrees from the University of Colorado, Boulder, all in aerospace engineering.

He is currently with the Naval Research Laboratory, Washington, DC. He has an extensive space hardware background where he has worked in the positions of Designer, Test Lead, P/L Integrator, Launch Site Coordinator, Vehicle Integration Manager, and Program Manager. He has worked both operational and R&D missions. Most recently, he was the WindSat Payload Program Manager, as well as the Civilian Deputy for the Navy METOC space program element. He is currently the Deputy Chief Engineer of the NPOESS environmental satellite program.

Gerald Golba (M'03) received the B.S. degree from The Ohio State University, Columbus, in 1985.

He is currently an electrical engineer working in the Space Electronics Development Branch, Naval Center for Space Technology, Naval Research Laboratory, Washington, DC. He has spent his entire career in the development of space system electronics including bus and payload components. He was the Electrical Systems Lead for the WindSat Payload.

Jeffrey Cleveland is a Computer Engineer with the Spacecraft Engineering Department, Naval Center for Space Technology, Naval Research Laboratory (NRL), Washington, DC. He has been with NRL for more than 15 years and has been involved with more than ten spacecrafts and space experiments, two of which are currently on-orbit and generating data. His experience has largely been with scientific spacecraft and experiments like the High Temperature Superconductor Space Experiment, the Microelectronics and Photonics Test Bed, and most recently, the WindSat payload. He is an expert in real-time software systems and has led the development of these systems for a number of his projects. He is also well qualified in the area of electronic system integration and testing. In addition to his work at NRL, he serves as an Adjunct Professor at the Northern Virginia Community College, Annandale.

Larry Choy received the B.A. degree from the University of California, Berkeley, and the Ph.D. degree from the University of New Hampshire, Durham, both in physics.

Since 1974, he has been with the Naval Research Laboratory, Washington, DC, doing applied physics research and program management on numerous satellite missions, both in the unclassified and classified domains. He is a currently a member of the Windsat ground-processing algorithm group. He joined the Windsat project about three years ago after completing a 7.5-year special assignment with the National Reconnaissance Office.

Richard M. Bevilacqua, photograph and biography not available at the time of publication.

Paul S. Chang (S'93–M'95–SM'03) received the B.S. degree in electrical engineering from Union College, Schenectady, NY, in 1988, and the Ph.D. degree in electrical engineering from the University of Massachusetts, Amherst, in 1994.

Since 1994, he has been with the Office of Research and Applications, National Environmental Satellite, Data and Information Service, National Oceanic and Atmospheric Administration, Camp Springs, MD. His primary interests have been active and passive microwave remote sensing of the ocean surface, with emphasis on the retrieval of the ocean surface wind vector. He is currently involved in the calibration and validation activities of WindSat (polarimetric radiometer) on Coriolis and SeaWinds (ku-band scatterometer) on ADEOS-II. He is also leading an effort to demonstrate and quantify the impacts of satellite remotely sensed ocean vector wind data on operational marine short-term forecasting and warnings.